ISSN 1344-3879
RIKEN-AF-NP-381

E1 Resonances in Neutron-Rich Nuclei within Phonon Damping Model[a]

N. D. Dang, V. K. Au, T. Suzuki, and A. Arima

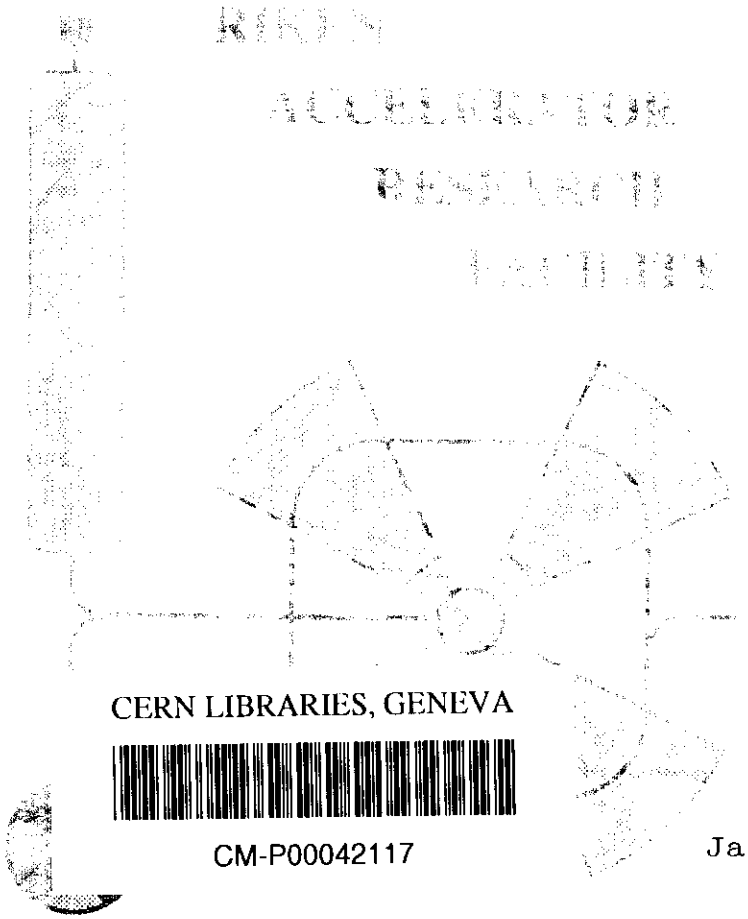

January 2001

The Institute of Physical and Chemical Research (RIKEN)
2-1 Hirosawa, Wako, Saitama 351-0198, Japan
TEL: (048)462-1111 FAX: (048)462-4642
e-mail: *username*@rikvax.riken.go.jp

E1 Resonances in Neutron-Rich Nuclei within Phonon Damping Model[a]

Nguyen Dinh Dang[1b], Vuong Kim Au[1], Toshio Suzuki[2], and Akito Arima[1,3]

[1] *RI-beam factory project office, RIKEN, 2-1 Hirosawa, Wako, Saitama 351-0198, Japan*

[2] *Department of Physics, College of Humanities and Sciences, Nihon University, Sakurajosui 3-25-40, Setagaya-ku, Tokyo 156-8550, Japan*

[3] *House of Councillors, Nagata-cho 2-1-1, Chiyoda-ku, Tokyo 100-8962, Japan*

Abstract

The quasiparticle representation of the phonon damping model (PDM) is developed to include the superfluid pairing correlations microscopically. The formalism is applied to calculate the photoabsorption and the electromagnetic (EM) differential cross sections of E1 excitations in neutron-rich oxygen and calcium isotopes. The calculated photoabsorption cross sections agree reasonably well with the available data for ^{16,18}O and ^{40,48}Ca. The results of calculations show that the change of the fraction of the E1 integrated strength in the region of pygmy dipole resonance (PDR) as a function of mass number A with increasing the neutron number N is in agreement with the recent experimental data, and does not follow the prediction by the simple cluster model. The EM differential cross sections obtained within PDM in this work show prominent PDR peaks below 15 MeV for ^{20,22}O in agreement with the recent experimental observation. It is also shown that, using low-energy RI beams at around 50 - 60 MeV/nucleon, one can observe clean and even enhanced PDR peaks without the admixture with the GDR in the EM differential cross sections of neutron-rich nuclei.

1 Introduction

I'm grateful to the organizers for inviting me to present a talk at this international symposium. My talk today is on the giant dipole resonances (GDR) and the excitations at its low-energy tail, called the pygmy dipole resonance (PDR), which appears in neutron-rich nuclei [1,2].

Although giant resonance is a subject of more than 50 years old, it continues to amaze us with new surprises. Those are the GDR in hot nuclei, multiple-

[a] Invited talk presented by N. Dinh Dang at the International Symposium on Nuclear Physics, December 18 - 22, 2000, Bhabha Atomic Research Centre, Mumbai, India

[b] On leave of absence from the Institute of Nuclear Science and Technique, VAEC, Hanoi, Vietnam. *Electronic addess*: dang@rikaxp.riken.go.jp

phonon giant resonance, the extraction of the high-lying tail of Gamow-Teller resonance (GTR), which recovers the missing part of the Ikeda sum rule, and PDR in neutron-rich nuclei. This is just to name a few of them. In the first ten years of the 21st century, we might be able to see the double GTR, or even giant resonances in hot exotic nuclei. So, this subject will surely continue to be very attractive.

Today I would like to show you how the features of these resonances, especially PDR and GDR, can be well described within a simple approach called the Phonon Damping Model (PDM), which has been proposed three years ago by Akito Arima and myself[3]. First, I would like to review briefly some successes of the PDM in the description of the damping of the GDR at finite temperature T and angular momentum J, in the study of double GDR (DGDR) and GTR. Next, I will show how the PDM is applied to calculate the photoabsorption and EM cross sections in neutron-rich oxygen and calcium isotopes. For this purpose we will develop the quasiparticle representation of the PDM to include microscopically the superfluid pairing correlation, which is important for the description of PDR.

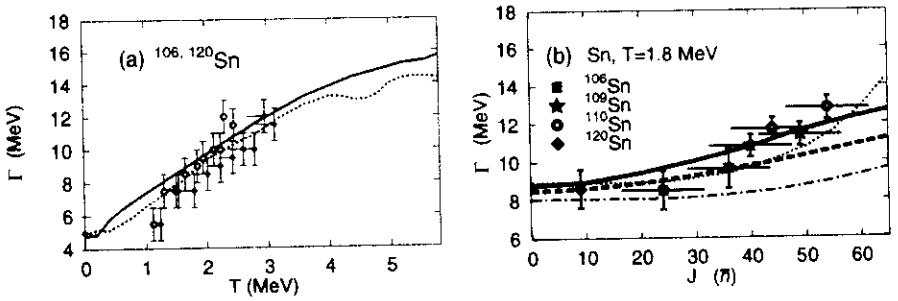

Figure 1: GDR width as a function of temperature T (a) and angular momentum J (b) in tin isotopes. In (a) the solid line is the width for ^{106}Sn, while the one for ^{120}Sn is given by the dotted line. The data points are taken from [7]. In (b) the thick solid and dashed lines are results obtained within PDM for ^{106}Sn and ^{120}Sn, respectively, while the corresponding results within the thermal fluctuation model are given by dotted and dash-dotted lines, respectively.

2 Brief review of some successes of PDM

The PDM has been proved to be quite successful in the description of the width and the shape of the GDR as a function of temperature T [3,4,5] and angular momentum J [6]. An example is shown in Fig. 1.

Shown in Fig. 2 is the prediction by PDM (solid line) in comparison with the result obtained within a microscopic theory which explicitly includes coupling to $2p2h$ configurations in terms of two-phonon configurations (dotted line) [9], and the experimental data (data points with errorbars) [10]. Again, the agreement between theory and experiment is quite reasonable. The PDM has

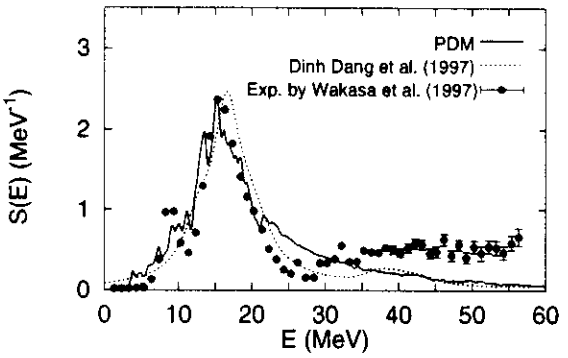

Figure 2: Strength functions of the GTR in 90Nb. See text for the notation.

also resolved the long-standing problem with the electromagnetic (EM) cross sections of the DGDR in ^{136}Xe and ^{208}Pb, in which the prediction by the non-interacting phonon picture underestimated significantly the observed DGDR cross sections by the LAND collaboration. The prediction using the strength functions obtained within PDM is given in Fig. 3 in comparison with the results of data analyses by LAND collaboration [11]. The agreement between the PDM prediction and the data is remarkable.

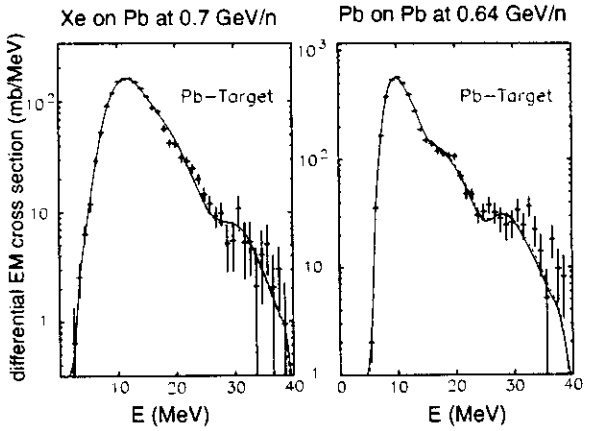

Figure 3: EM cross sections of GDR and DGDR for ^{136}Xe and ^{208}Pb. The solid lines are theoretical predictions, in which the DGDR strength functions within PDM are used. The data points are results of the LAND collaboration [11]. The dashed lines show the best fit using χ^2. The theoretical results have been folded with the detector response by K. Boretzky.

3 Quasiparticle representation of phonon damping model

The quasiparticle representation of the PDM Hamiltonian [3,4] is obtained by adding the superfluid pairing interaction in it and expressing the particle (p) and hole (h) creation and destruction operators, $a_s^\dagger$ and a_s ($s = p, h$), in terms of the quasiparticle operators, $\alpha_s^\dagger$ and α_s, using the Bogolyubov's canonical transformation. As a result, the PDM Hamiltonian for the description of Eλ

excitations can be written in spherical basis as

$$H = \sum_{jm} \epsilon_j \alpha^\dagger_{jm} \alpha_{jm} + \sum_{\lambda\mu i} \omega_{\lambda i} b^\dagger_{\lambda\mu i} b_{\lambda\mu i} \ + \frac{1}{2} \sum_{\lambda\mu i} \frac{(-)^{\lambda-\mu}}{\hat{\lambda}} \sum_{jj'} f^{(\lambda)}_{jj'} \times$$

$$\left\{ u^{(+)}_{jj'} \left[A^\dagger_{jj'}(\lambda\mu) + A_{jj'}(\lambda\tilde{\mu}) \right] + v^{(-)}_{jj'} \left[B^\dagger_{jj'}(\lambda\mu) + B_{jj'}(\lambda\tilde{\mu}) \right] \right\} \left(b^\dagger_{\lambda\mu i} + b_{\lambda\tilde{\mu} i} \right) \ , \quad (1)$$

where $\hat{\lambda} = \sqrt{2\lambda + 1}$. The first term at the right-hand side (RHS) of Hamiltonian (1) corresponds to the independent-quasiparticle field. The second term stands for the phonon field described by phonon operators, $b^\dagger_{\lambda\mu i}$ and $b_{\lambda\mu i}$, with multipolarity λ, which generate the harmonic collective vibrations such as GDR. Phonons are ideal bosons within PDM, i.e. they have no fermion structure. The last term is the coupling between quasiparticle and phonon fields, which is responsible for the microscopic damping of collective excitations.

In Eq. (1) the following standard notations are used

$$A^\dagger_{jj'}(\lambda\mu) = \sum_{mm'} \langle jmj'm'|\lambda\mu\rangle \alpha^\dagger_{jm} \alpha^\dagger_{j'm'} \ ,$$

$$B^\dagger_{jj'}(\lambda\mu) = -\sum_{mm'} (-)^{j'-m'} \langle jmj'-m'|\lambda\mu\rangle \alpha^\dagger_{jm} \alpha_{j'm'} \ , \quad (2)$$

with $(\lambda\tilde{\mu}) \longleftrightarrow (-)^{\lambda-\mu}(\lambda-\mu)$. Functions $u^{(+)}_{jj'} \equiv u_j v_{j'} + v_j u_{j'}$ and $v^{(-)}_{jj'} \equiv u_j u_{j'} - v_j v_{j'}$ are combinations of Bogolyubov's u and v coefficients. The quasiparticle energy ϵ_j is calculated from the single-particle energy E_j as

$$\epsilon_j = \sqrt{(\tilde{E}_j - E_{\rm F})^2 + \Delta^2} \ , \qquad \tilde{E}_j \equiv E_j - G v_j^2, \quad (3)$$

where the pairing gap Δ and the Fermi energy $E_{\rm F}$ are defined as solutions of the BSC equations (See, e.g., [12]) The operators in (2) and their hermitian conjugates satisfy the following commutation relations within the ensemble average

$$\left\langle [A_{jj'}(\lambda\mu), A^\dagger_{j_1 j'_1}(\lambda'\mu')] \right\rangle = (1 - n_j - n_{j'}) \delta_{\lambda\lambda'} \delta_{\mu\mu'} \left[\delta_{jj_1} \delta_{j'j'_1} + (-)^{j'-j+\lambda} \delta_{jj'_1} \delta_{j'j_1} \right] \ , \quad (4)$$

$$\left\langle [B_{jj'}(\lambda\mu), B^\dagger_{j_1 j'_1}(\lambda'\mu')] \right\rangle = (n_{j'} - n_j) \delta_{\lambda\lambda'} \delta_{\mu\mu'} \delta_{jj_1} \delta_{j'j'_1} \ , \quad (5)$$

where it is assumed that $\langle\alpha_j^\dagger\alpha_{j'}\rangle = 0$ if $j \neq j'$. The quantity $n_j = \langle\alpha_j^\dagger\alpha_j\rangle$ is the quasiparticle occupation number defined in within the grand canonical ensemble at a given temperature $T = \beta^{-1}$. It becomes zero at $T = 0$.

The equation for the propagation of the GDR phonon, which is damped due to coupling to quasiparticle field, is derived below making use of the double-time Green's function method [13]. For this purpose, the following double-time Green's functions are introduced similarly to the case without pairing within PDM[3]. They are i) The phonon propagation: $G_{\lambda i}(t-t') = \langle\langle b_{\lambda\tilde{\mu}i}(t); b^\dagger_{\lambda\mu i}(t')\rangle\rangle$, ii) The forward-going transition between quasiparticle pair and phonon: $\mathcal{G}^A_{jj';\lambda i}(t-t') = \langle\langle A_{jj'}(\lambda\tilde{\mu})(t); b^\dagger_{\lambda\mu i}(t')\rangle\rangle$, iii) The backward-going transition between quasiparticle pair and phonon: $\mathcal{G}^{A^\dagger}_{jj';\lambda i}(t-t') = \langle\langle A^\dagger_{jj'}(\lambda\mu)(t); b^\dagger_{\lambda\mu i}(t')\rangle\rangle$, iv) The forward-going transition between scattering-quasiparticle pair and phonon: $\mathcal{G}^B_{jj';\lambda i}(t-t') = \langle\langle B_{jj'}(\lambda\tilde{\mu})(t); b^\dagger_{\lambda\mu i}(t')\rangle\rangle$, v) The backward-going transition between scattering-quasiparticle pair and phonon: $\mathcal{G}^{B^\dagger}_{jj';\lambda i}(t-t') = \langle\langle B^\dagger_{jj'}(\lambda\mu)(t); b^\dagger_{\lambda\mu i}(t')\rangle\rangle$. Here the conventional notation of the double-time Green's functions [13] is used. Following the standard procedure of deriving the equation for the double-time Green's function with respect to the Hamiltonian (1), and using of the commutation relations (4) and (5), one obtains a closed set of equations for these Green's functions. Making the Fourier transform into the energy plane E, and expressing all the Green functions in the set in terms of the one-phonon propagation Green function, we obtain the equation for the latter, $G_{\lambda i}(E)$, in the form

$$G_{\lambda i}(E) = \frac{1}{2\pi}\frac{1}{E - \omega_{\lambda i} - P_{\lambda i}(E)} , \tag{6}$$

where the explicit form of the polarization operator $P_{\lambda i}(E)$ is

$$P_{\lambda i}(E) = \frac{1}{\lambda^2}\sum_{jj'}[f^{(\lambda)}_{jj'}]^2\left[\frac{(u^{(+)}_{jj'})^2(1-n_j-n_{j'})(\epsilon_j+\epsilon_{j'})}{E^2-(\epsilon_j+\epsilon_{j'})^2}\right.$$

$$\left.-\frac{(v^{(-)}_{jj'})^2(n_j-n_{j'})(\epsilon_j-\epsilon_{j'})}{E^2-(\epsilon_j-\epsilon_{j'})^2}\right]. \tag{7}$$

The phonon damping $\gamma_{\lambda i}(\omega)$ (ω real) is obtained as the imaginary part of the analytic continuation of the polarization operator $P_{\lambda i}(E)$ into the complex energy plane $E = \omega \pm i\varepsilon$. Its final form is

$$\gamma_{\lambda i}(\omega) = \frac{\pi}{2\lambda^2}\sum_{jj'}[f^{(\lambda)}_{jj'}]^2\Big\{(u^{(+)}_{jj'})^2(1-n_j-n_{j'})[\delta(E-\epsilon_j-\epsilon_{j'})-\delta(E+\epsilon_j+\epsilon_{j'})]-$$

$$(v_{jj'}^{(-)})^2(n_j - n_{j'})[\delta(E - \epsilon_j + \epsilon_{j'}) - \delta(E + \epsilon_j - \epsilon_{j'})]\Big\}. \tag{8}$$

At zero temperature all the quasiparticle occupation numbers n_j are zero, so the factor $1 - n_j - n_{j'}$ becomes 1, while the last terms at the RHS of Eqs. (7) and (8), which contain $(v_{jj'}^{(-)})^2$, vanish. It is also worth noticing that the contribution to the GDR of the term $\sim \delta(E + \epsilon_j + \epsilon_{j'})$ due to backward-going process should be negligible as its maximum is at $-(\epsilon_j + \epsilon_{j'}) < 0$.

The energy $\bar{\omega}$ of giant resonance (damped collective phonon) is found as the pole of the Green's function (6), i.e. as the solution of the following equation

$$\bar{\omega} - \omega_{\lambda i} - P_{\lambda i}(\bar{\omega}) = 0 \ . \tag{9}$$

The width Γ_λ of giant resonance is calculated as twice of the damping $\gamma_\lambda(\omega)$ at $\omega = \bar{\omega}$, i.e.

$$\Gamma_\lambda = 2\gamma_\lambda(\bar{\omega}), \tag{10}$$

where $\lambda = 1$ corresponds to the GDR. As has been discussed previously [3,4], the presence of polarization operator (7) due to *ph* – phonon coupling in the last term of the RHS of Hamiltonian (1) and the property of the double-time Green's function, which allows the analytic continuation into the complex energy plan, allows the damping to be calculated in an explicit and microscopic way given by Eq. (8).

The line shape of the GDR is described by the strength function $S_{\rm GDR}(\omega)$, which is derived from the spectral intensity in the standard way using the analytic continuation of the Green function (6) [14] and by expanding the polarization operator (7) around $\bar{\omega}$ [13]. The final form of $S_{\rm GDR}(\omega)$ is [3]

$$S_{\rm GDR}(\omega) = \frac{1}{\pi} \frac{\gamma_{\rm GDR}(\omega)}{(\omega - \bar{\omega})^2 + \gamma_{\rm GDR}^2(\omega)} \ . \tag{11}$$

Note that function (11) has only a Breit-Wigner-like form since the damping $\gamma_{\rm GDR}(\omega)$ depends on the energy ω. The photoabsorption cross section $\sigma(E_\gamma)$ is calculated from the strength function $S_{\rm GDR}(E_\gamma)$ as

$$\sigma(E_\gamma) = c_1 S_{\rm GDR}(E_\gamma) E_\gamma \ , \tag{12}$$

where $E_\gamma \equiv \omega$ is used to denote the energy of γ-emission. The normalization factor c_1 is defined so that the total integrated photoabsorption cross section $\sigma = \int \sigma(E_\gamma) dE_\gamma$ satisfies the GDR sum rule $\mathrm{SR}_{\rm GDR}$, hence

$$c_1 = \mathrm{SR}_{\rm GDR} \Big/ \int_0^{E_{\rm max}} S_{\rm GDR}(E_\gamma) E_\gamma dE_\gamma \ . \tag{13}$$

In heavy nuclei with $A \geq 40$, the GDR exhausts the Thomas-Reich-Kuhn (TRK) sum rule $\mathrm{SR_{GDR}} = \mathrm{TRK} \equiv 60\ NZ/A$ (MeV·mb) at the upper integration limit $E_{\max} \simeq 30$ MeV, and exceeds TRK ($\mathrm{SR_{GDR}} > \mathrm{TRK}$) at $E_{\max} > 30$ MeV due to the contribution of exchange forces. In some light nuclei, such as ^{16}O, the observed photoabsorption cross section exhausts only around 60% of TRK up to $E_{\max} \simeq 30$ MeV [1].

According to [15,16], the EM cross section σ_{EM} is calculated from the corresponding photoabsorption cross section $\sigma(E_\gamma)$ and the photon spectral function $N(E_\gamma)$ as

$$\sigma_{\mathrm{EM}} = \int N(E_\gamma)\sigma(E_\gamma)dE_\gamma, \qquad N(E_\gamma) = 2\pi \int_{b_{\min}}^{\infty} \mathrm{e}^{-m(b)} N(E_\gamma, b) b db. \quad (14)$$

The expression for the spectrum $N(E_\gamma, b)$ of virtual photon from a stationary target as seen by a projectile moving with a velocity $\beta = v/c$ at impact parameter b is also given in [16]. The mean number of photons absorbed by the projectile is calculated as $m(b) = \int_{E_{\min}}^{\infty} N(E_\gamma, b)\sigma(E_\gamma)dE_\gamma$.

4 Numerical results

The calculations of photoabsorption and EM cross sections have been carried out for oxygen isotopes with $A = 16$, 18, 20, 22, and 24, and for calcium isotopes with $A = 40$, 42, 44, 46, 48, 50, 52, and 60. The calculations employ the spherical-basis single-particle energies E_j obtained within the Hartree-Fock method using the SGII interaction [17]. The principal point, which is maintained throughout our study of GDR in neutron-rich nuclei, is that we extrapolate the description of closed-shell nuclei within PDM to the region of neutron open-shell nuclei, assuming they are all spherical. This means that the two PDM parameters ω_λ ($\lambda = 1$) and $f_1 = f^{(1)}_{jj'}$ for all ph indices ($j = p, j' = h$) are chosen so that the values of GDR energy $E_{\mathrm{GDR}} \equiv \bar{\omega}$ and width Γ_{GDR}, calculated from Eqs. (9) and (10) for ^{16}O and ^{40,48}Ca, reproduce their corresponding experimental values $E^{\mathrm{exp}}_{\mathrm{GDR}}$ and $\Gamma^{\mathrm{exp}}_{\mathrm{GDR}}$ (See [3] for more details about the procedure of choosing parameters within PDM). The values of PDM parameters for ^{16}O are then fixed in calculations for all oxygen isotopes ($N \geq Z$). For calciums, we used the parameters selected for ^{40}Ca in calculations for isotopes with $20 \leq N < 28$, and those selected for ^{48}Ca in calculations with $N \geq 28$. The neutron pairing gap Δ_{n} is adjusted around the general trend $12/\sqrt{A}$ of the observed pairing gaps in stable nuclei. The adjustment is necessary to keep the GDR energy remain nearly unchanged with increasing N as the values of parameters ω_1 and f_1 are kept fixed for three groups of isotopes $^{16-24}$O, $^{40-46}$Ca, and $^{48-60}$Ca separately. For ^{16}O, we found the PDM parameters $\omega_1 = 22.5$

MeV and $f_1 = 0.2850$ MeV, which yield the GDR energy $E_{\rm GDR} = 23.7$ MeV and width $\Gamma_{\rm GDR} = 5.85$ MeV. For ^{40}Ca (^{48}Ca), the selected values of PDM parameters are $\omega_1 = 19.51$ MeV and $f_1 = 0.1396$ MeV (0.1867 MeV), which lead to $E_{\rm GDR} = 19.6$ MeV (19.4 MeV) and $\Gamma_{\rm GDR} = 4.9$ MeV (7.15 MeV). The selected values of Δ are plotted as black squares against the neutron number N in Fig. 4, which shows that they are within the range of experimental systematic for neutron pairing gaps in stable nuclei [18]. The δ-function in the damping (8)

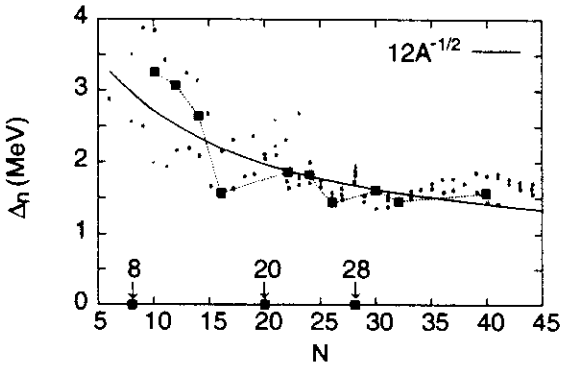

Figure 4: Selected neutron pairing gaps $\Delta_{\rm n}$ (black squares) in comparison with the experimental systematic for stable nuclei (grey circles) and the trend $\Delta = 12/\sqrt{A}$ (solid line).

is smoothed out using the representation $\delta(x) = [(x - i\varepsilon)^{-1} - (x + i\varepsilon)^{-1}]/(2\pi i)$ with $\varepsilon = 0.5 \sim 1$ MeV. The averaged quantities such as the energy-weighted sum (EWS) of E1 strength and shape of GDR do not change significantly using $0.1 \leq \varepsilon \leq 1.5$ MeV. The results discussed below are obtained in calculations using the value of the smearing parameter ε equal to 0.5 MeV for oxygens, and 1 MeV for calciums. The normalization factor c_1 from Eq. (13) is defined as follows. For ^{16}O, the factor c_1 is chosen so that $\mathrm{SR}_{\rm GDR}$ reproduces the experimental EWS of E1 strength, which amounts to 54% of TRK with $E_{\rm max} = 29$ MeV. For other oxygen isotopes, c_1 is found so that 100% of TRK is exhausted at $E_{\rm max} = 50$ MeV. For calciums, c_1 is defined so that the EWS of E1 strength fulfills 100% of TRK at $E_{\rm max} = 28$ MeV for $40 \leq A < 48$, and 156±3% of TRK at $E_{\rm max} = 50$ MeV for $A \geq 48$. This criterion is an extrapolation of the experimental values of TRK fraction exhausted in the photoabsorption cross sections for ^{40,48}Ca.

Shown in Figs. 5 and 6 are the photoabsorption cross sections $\sigma(E_\gamma)$, which have been obtained within PDM for oxygen and calcium isotopes, respectively. The shapes of the photoabsorption cross section calculated for stable isotopes ^{16,18}O and ^{40,48}Ca are found in overall reasonable agreement with available experimental data [1,19,20] as shown in the left panels of Fig. 7 ((a) - (d)). This agreement is obviously better than those given by several elaborated models shown in the right panels of Fig. 7 ((e) - (h)), namely the large-scale shell model (LSSM) [21] using Warburton-Brown interaction WB10 (thin solid and

thin dashed lines in (e) and (f) with $T_< = 1$ and $T_> = 2$ denoting two isospin components of GDR in ^{18}O), the surface coupling model (SCM) using the coupling of ph configurations with surface phonon [22] (dotted lines in (e) and (g)), the second RPA (SRPA) [23] (thick dashed line in (g)), and a microscopic model including $1p1h\otimes$phonon plus continuum (phPC) [24] (dash-dotted lines in (g) and (h)). Experimental photoabsorption cross sections for other oxygens and calciums in the chains considered here are not available at present. It

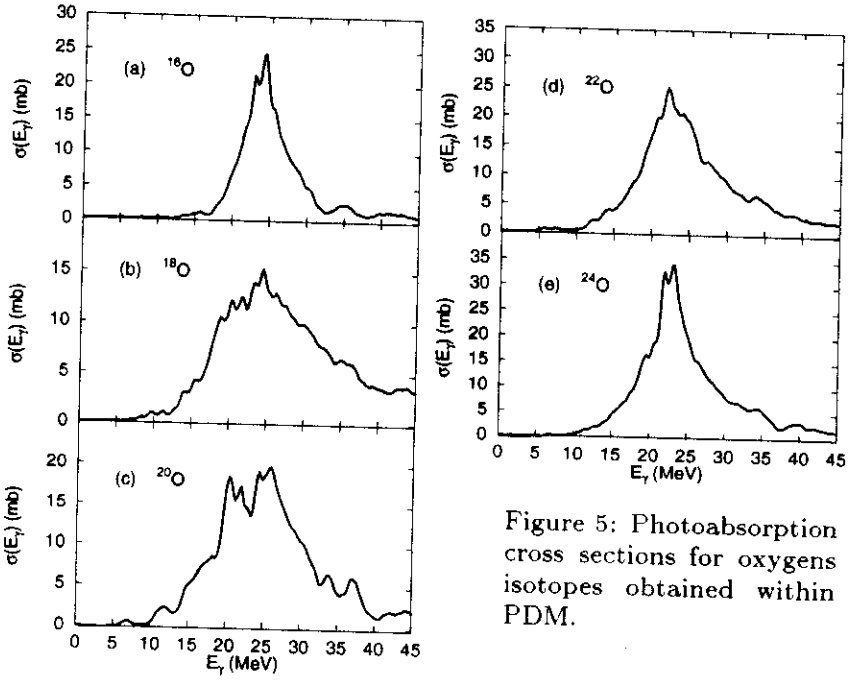

Figure 5: Photoabsorption cross sections for oxygens isotopes obtained within PDM.

is seen from Figs. 5 and 6 that the GDR becomes broader for isotopes with $N > Z$. Its width is particularly large for isotopes between the double closed shell ones, such as ^{18,20}O, or ^{52}Ca. The increase of GDR spreading enhances both of its low- and high-energy tails. In the region $E_\gamma \leq 15$ MeV, some weak structure of PDR is visible for ^{18,20,22}O. In the rest of isotopes under study, except for an extension of the GDR tail toward lower-energy, there is no visible structure of PDR. This is in contrast with the results by some other approaches, where the GDR spreading width is not explicitly calculated, such as the one in [25] or the LSSM [21]. In these approaches, prominent peaks in the GDR strength function are obtained in the region below 10 - 15 MeV in ^{20,22,24}O [21,25] and ^{60}Ca [25]. We note, however, that neither [25] nor LSSM can describe correctly the GDR shape in stable double-closed shell nuclei ^{16}O and ^{40,48}Ca.

The fractions of the EWS of strength exhausted by the low-energy tail

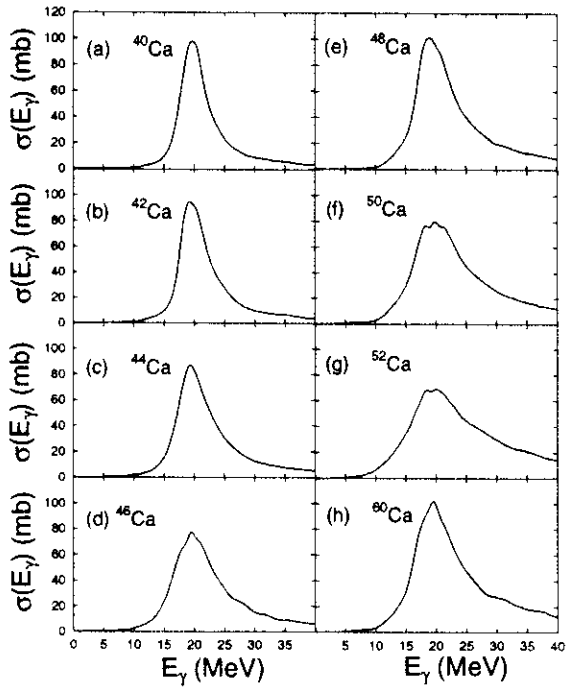

Figure 6: Photoabsorption cross sections for calcium isotopes obtained within PDM.

of GDR are shown in Figs. 8. The trend obtained within PDM for oxygens reproduces the one observed in the recent experiments at GSI [2], which shows a clear deviation from the prediction by the cluster sum rule (CSR) (also called as molecular dipole sum rule) [26]. In calciums, where the GDR is more collective and exhausts 100% of TRK already below $E_\gamma = 30$ MeV, the prediction by CSR is fairly reproduced up to $A = 52$ using $E_{\max} = 16$ MeV. We notice that the fractions of EWS of PDR strength are not zero even for double closed-shell nuclei ^{16}O and ^{40,48}Ca because the low-energy tail in photoabsorption cross sections, which are experimentally observed and obtained as results of calculations within PDM, spreads below $E_\gamma = 15$ MeV also for these nuclei. The EWS of strength between 5 and 10 MeV obtained within PDM for ^{48}Ca is 0.52% of TRK to be compared with the value of 0.29 ± 0.04 % of TRK extracted in the recent high-photon scattering experiments [27]. The agreement between the PDM prediction and the experimental data for the photoabsorption cross sections as well as for the EWS of PDR strength suggests that the mechanism of the damping of PDR is dictated by the coupling between the GDR phonon and noncollective *ph* excitations rather than by the oscillation of a collective neutron excess against the core. Strong pairing correlations also prevent the weakly bound neutrons to be decoupled from the rest of the system [28]. Only

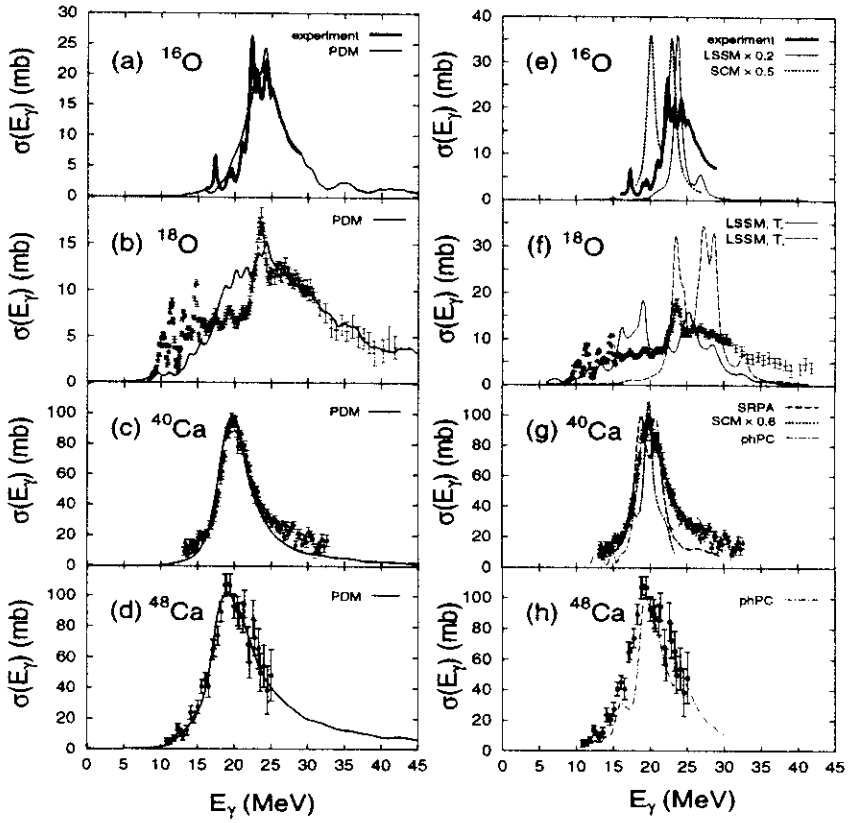

Figure 7: Photoabsorption cross sections for ^{16,18}O and ^{40,48}Ca obtained within PDM (left panels) and within other models mentioned in the text (right panels) in comparison with experimental data from [1] (thick solid line in (a) and (e)), [1] ((b) and (f)), [19] ((c) and (g)), and [20] ((d) and (h)).

when the GDR is very collective so that it can be well separated from the neutron excess, the picture of PDR damping becomes closer to the prediction by the CM.

The photon spectral function $N(E_\gamma)$ in the EM differential cross section $d\sigma_{\rm EM}/dE_\gamma$ (Eq. (14)) contains an exponentially decreasing factor $e^{-m(b)}$ with increasing E_γ. It is clear that this behavior enhances the low-energy part of the E1 strength in the EM differential cross section. Therefore, the latter can be used as a magnifying glass for the structure of PDR. These EM differential cross sections obtained within PDM are shown in Figs. 9 and 10 for oxygens and calciums, respectively. The calculations were carried out for ^{208}Pb target at various projectile energies as shown in these figures. All the values shown in the figures have been normalized so that the integrated EM cross sections up to 50 MeV correspond to 100% of TRK. The PDR shows up in the EM

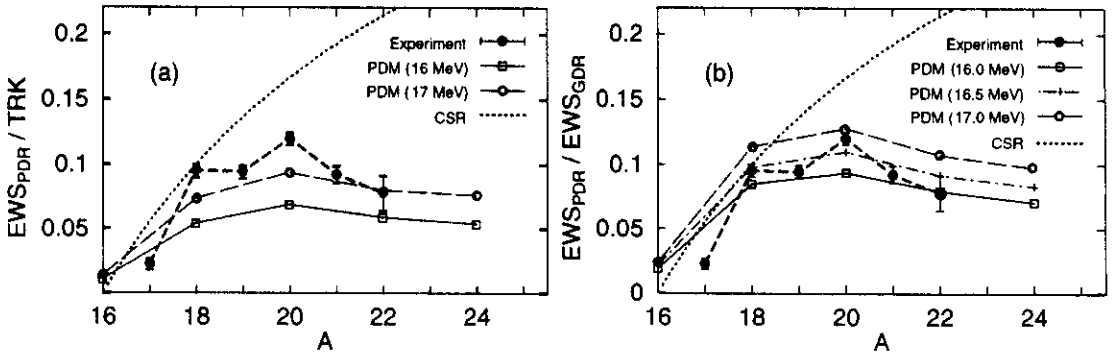

Figure 8: EWS of PDR strength up to excitation energy $E_{\max}$ for oxygens. Results obtained within PDM with $E_{\max} = 16$, 16.5, and 17 MeV are displayed as open boxes connected with solid line, crosses connected with dash-dotted line, and open circles connected with thin dashed line, respectively. In (a) the PDM results are shown in units of TRK, while in (b) they are in units of the total GDR strength integrated up to 30 MeV. Experimental data (in units of TRK), obtained with $E_{\max} = 15$ MeV, are shown by full circles connected with thick dashed line. The dotted line is the prediction by the cluster sum rule (CSR) (in units of TRK).

cross sections of all neutron-rich isotopes, especially for ^{20,22}O, where a well isolated peak located at around 7 MeV is clearly seen. The PDR becomes depleted when the neutron number approaches a magic number (where the GDR is most collective) as can be seen in calciums when N increases from 20 to 28. Therefore, the decrease of PDR strength in ^{24}O and ^{60}Ca can be understood as the depletion on the way toward the next magic number ($N = 28$ and 50, respectively). It is also important to point out the impact on the EM differential cross section by the behavior of the photon spectral function $N(E_\gamma)$ at various projectile energies. Indeed, because of the behavior of $N(E_\gamma)$, the decrease of the projectile energy from 700 MeV/nucleon to 300 MeV/nucleon strongly reduces the EM cross section in the GDR region (above 10 MeV), but leaves the PDR almost intact, as can be seen in Fig. 9. A further decrease of projectile energy to 50 MeV/nucleon suppresses completely the GDR peak and even enhances the PDR peak in some very neutron-rich nuclei ^{20,22,24}O or ^{52}Ca (dash-dotted lines in Figs. 9 and 10). This observation shows that, using high-intensity RI beams at low energies of around 50 – 60 MeV/nucleon, one may be able to observe a rather clean and sharp PDR peak in ^{20,22}O in the region around 7 MeV, and probably a broad peak below 5 MeV in ^{52}Ca. The preliminary results of recent measurements of EM differential cross sections for E1 excitations in ^{20,22}O at GSI [2] have shown a peak-like structure at $E_\gamma \simeq 8$ MeV and another bump in the region between 12 and 16 MeV. Our results for PDR from Fig. 9 (c) and (d) are in qualitative agreement with the GSI data,

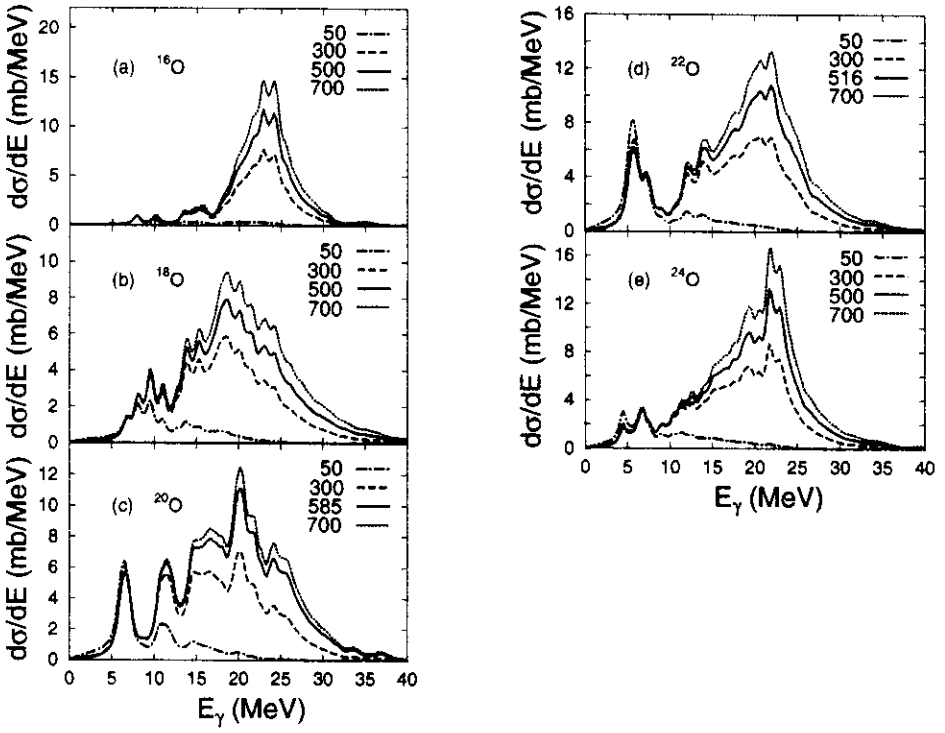

Figure 9: Electromagnetic cross sections of E1-excitations within PDM for oxygens on ^{208}Pb target. Different lines display results obtained at different projectile energies, whose values (in MeV/nucleon) are indicated in the panels.

which have been, however, presented with the detector response folded in.

5 Conclusions

I have shown how the E1 resonances in neutron-rich oxygen and calcium isotopes are described within the quasiparticle representation of the PDM. From the results obtained within PDM, the following conclusions can be drawn:

1) The PDM gives the GDR shapes in ^{16,18}O and ^{40,48}Ca in reasonable agreement with the experimental data.

2) The change of the fraction of E1 integrated strength in the region of PDR as a function of A with increasing N is in agreement with the GSI preliminary data. This suggests that the authentic damping mechanism of giant resonance is the result of coupling between collective phonon and non-collective *ph* configurations.

3) The EM differential cross sections may serve as a better probe for PDR as compared to the photoabsorption cross section. The former show prominent PDR peaks below 15 MeV for ^{20,22}O in agreement with the experimental

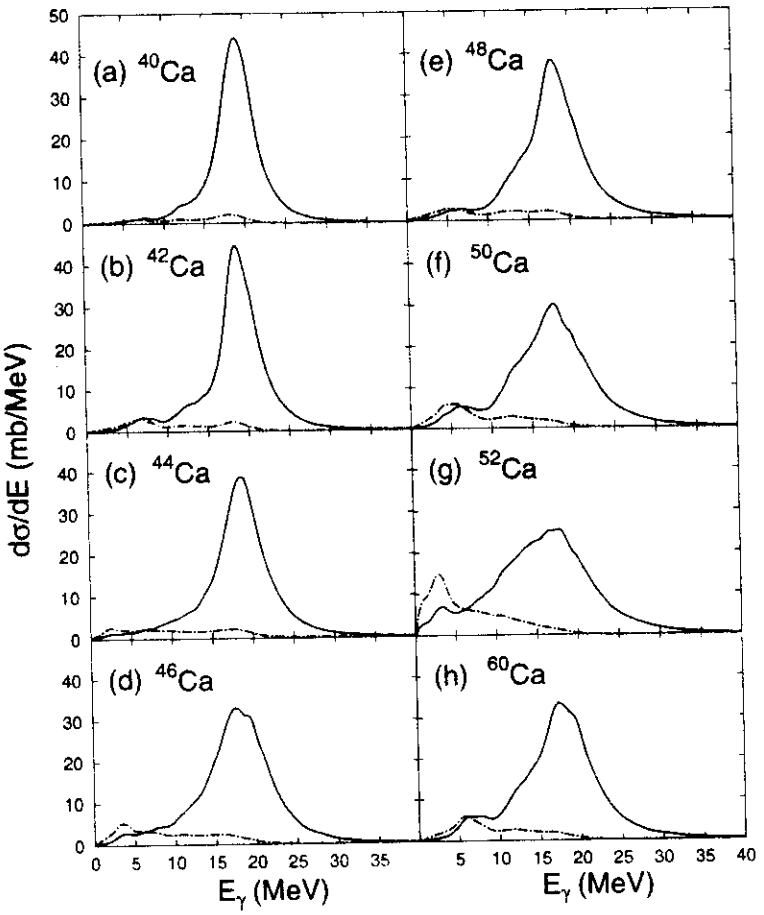

Figure 10: Electromagnetic cross sections of E1-excitations within PDM for calciums on ^{208}Pb target at 500 MeV/nucleon (solid lines) and 50 MeV/nucleon (dash-dotted lines).

observation.

4) Using low-energy (but intensive) RI beams of energy around 50 - 60 MeV/nucleon, one can observe clean and even enhanced PDR peaks without admixture with the GDR in the EM differential cross sections of neutron-rich nuclei.

References

1. J.G. Woodworth et al., Phys. Rev. **C 19** (1979) 1667.
2. T. Aumann et al., GSI Scientific Report 1999 (2000) 27.
3. N. Dinh Dang and A. Arima, Phys. Rev. Lett. **80** (1998) 4145, Nucl. Phys. **A 636** (1998) 427.

4. N. Dinh Dang. K. Tanabe, and A. Arima, Phys. Rev. **C 58** (1998) 3374, Nucl. Phys. **A 645** (1999) 536.
5. N. Dinh Dang et al., Phy. Rev. **C 61** (2000) 027302
6. N. Dinh Dang, Description of single- and multiple-phonon giant dipole resonances within the phonon damping model, Invited talk at the international conference on giant resonances GR2000, Osaka, June 12 - 15, 2000, to appear in Nucl. Phys. A; N. Dinh Dang, A. Ansari, and A. Arima, Angular-momentum effect on the width of hot giant dipole resonance within the phonon damping model, Preprint RIKEN-AF-NF 361 (2000) (10 pages) (submitted).
7. T. Baumann et al., Nucl. Phys. **A 635** (1998) 428, **A649** (1999) 173c.
8. N. Dinh Dang, T. Suzuki, and A. Arima, Description of Gamow - Teller resonance within the phonon damping model, Preprint RIKEN-AF-NF 377 (2000) (11 pages) (submitted).
9. N. Dinh Dang et al., Nucl. Phys. **A 621** (1997) 719.
10. T. Wakasa et al., Phys. Rev. **C 55** (1997) 2909.
11. K. Boretzky, private communication (2000).
12. A.V. Ignatyuk, Statistical properties of excited atomic nuclei (Moscow, Energoatomizdat, 1983).
13. D.N. Zubarev, Sov. Phys. Uspekhi **3** (1960) 320.
14. N.N. Bogolyubov and S.V. Tyablikov, Soviet Phys.-Doklady **4** (1959) 60.
15. W. J. Llope and P. Braun-Muzinger, Phys. Rev. C **41**, (1990) 2644.
16. I.A. Pshenichnov *et al.*, Phys. Rev. C **60** (1999) 044901.
17. N. Van Giai and H. Sagawa, Nucl. Phys. **A 371** (1981) 1.
18. A. Bohr and B.R. Mottelson, Nuclear Structure, vol. 1 (New York, Benjamin, 1969) p. 170.
19. J. Ahrens et al., Nucl. Phys. **A 251** (1975) 479.
20. G.J. O'keefe et al., Nucl. Phys. **A 649** (1987) 239.
21. H. Sagawa and T. Suzuki, Phys. Rev. **C 59** (1999) 3116.
22. P.F. Bortignon and R.A. Borglia, Nucl. Phys. **A 371** (1981) 405.
23. S. Nishizaki and J. Wambach, Phys. Lett. **B 349** (1995) 7.
24. S. Kamerdzhiev, J. Speth, and G. Tertychny, Nucl. Phys. **A 624** (1997) 328.
25. P.-G. Reinhard, Nucl. Phys. **A 649** (1999) 305c.
26. Y. Alhassid, M. Gai, and G.F. Bertsch, Phys. Rev. Lett. **49** (1982) 1482.
27. T. Hartmann et al., Phys. Rev. Lett. **85** (2000) 274.
28. S. Mizutori et al., Phys. Rev. **C 61** (2000) 044326.